Mon. Not. R. Astron. Soc. **264,** 597–603 (1993)

Geometrical effects in models of OH/IR-star masers

Huib Jan van Langevelde★ and Marco Spaans
Sterrewacht Leiden, PO Box 9513, 2300 RA Leiden, The Netherlands

Accepted 1993 March 27. Received 1993 March 5

ABSTRACT

We use a model presented earlier to address several outstanding questions about the 1612-MHz masers in OH/IR stars. First, we explore the parameter values for modelling the masers, and show that the appearance of the masers has no strong dependence on the shell thickness, OH density or velocity distribution of the OH molecules. Secondly, we examine the possible mismatch between angular size and phase-lag size, which may affect distance estimates. Such an effect may arise because of the anisotropy of the maser emission, but is found to be small. Finally, we discuss the presence of maser emission of high brightness temperature in the blueshifted peak, and show that it is indeed possible that this effect is caused by amplified stellar emission.

Key words: line: profiles – masers – radiative transfer – circumstellar matter – stars: distances – radio lines: stars.

1 INTRODUCTION

The mechanism for producing 1612-MHz OH masers in circumstellar shells is relatively well understood (see Cohen 1989, or Elitzur 1992, for a review). The process that excites the maser is pinned down to a radiative pump within the low-energy rotational transitions of the OH molecule (Elitzur, Goldreich & Scoville 1976). In Spaans & van Langevelde (1992, hereafter Paper I), we showed that we could reproduce the observed spectra by using a model for the two-dimensional radiative transfer with standard physical parameters. For the physical parameters we used estimates of the OH density and temperature from previous model calculations (Netzer & Knapp 1987). Here we explore further the model presented in Paper I.

1.1 The problems that are addressed

Three different subjects are addressed in this paper.

(i) *The conditions for the occurrence of circumstellar OH masers.* In Paper I, a model was presented for one particular set of the input parameters. Here we vary these parameters and study their effects on the appearance of the maser. This results in a phenomenological study of the model; a discussion of the physical (and chemical) conditions in circumstellar shells is beyond the scope of this paper.

(ii) *Phase lags.* We also use COHERENCE, the code that was presented in Paper I, to discuss the assumptions necessary to make phase-lag distance measurements to OH/IR stars (see Herman & Habing 1985a for a review, or van Langevelde, van der Heiden & van Schooneveld 1990). When the variability of the peaks of an OH/IR star is monitored accurately, a phase lag can be measured between the blue- and the redshifted peak, which has a direct relation with the linear size of the circumstellar shell. By combining this linear size with angular size measurements, the distance to OH/IR stars has been determined. It has often been argued that the only assumption in this method is that of spherical symmetry, which seems justified in a statistical sense, if not for individual OH/IR stars. However, this condition is necessary but not sufficient (van Langevelde et al. 1990). Because the maser emits non-isotropically, radiation in different directions may originate from different locations in the shell, especially from different radii, and this may bias the phase-lag distance.

(iii) *Amplified stellar emission.* Another feature studied with COHERENCE is the presence of amplified stellar emission. VLBI observations of the blueshifted peak of the OH spectrum often show a spot of high brightness temperature which has no counterpart in the redshifted peak. The hypothesis is that this spot is the amplified stellar image. For the specific line of sight to the stellar surface, the maser mechanism is triggered by photons originating from the star. As a counter-argument, the fact that on average the blue- and redshifted peaks have equal flux densities has been used. This is not a constraint, however, on the existence of an amplified stellar image; although the flux densities from both peaks may be similar, the intensity distributions may be

★ E-mail (internet): vlangeve@strwchem.LeidenUniv.nl.

different. We use a modified version of COHERENCE to investigate the presence of amplified stellar images in OH masers.

We will treat these three subjects separately in Sections 2–4. In Section 5 the overall conclusions will be presented.

1.2 The code

The program COHERENCE, developed to model radiative transfer in circumstellar masers, is a Monte Carlo-type code. As discussed in Paper I, there are some limitations to the use of such a code. At the moment, only OH/IR stars with limited OH luminosity can be modelled, because the step-size in the code may not exceed $l_{\rm mfp}$, the mean free path in the medium. Because the computer time required scales with the number of steps to the third power, arbitrarily strong masers cannot be modelled.

Another limitation arises from the $\sqrt{N}$ statistics of the Monte Carlo method. Even when we model the local radiative transfer with proper resolution, we may not have the ability to study an observable (spectrum or brightness distribution) with high resolution, because too few photon packages contribute to the bins that we want to study. For example, when the presence of maser hotspots is discussed, predictions for the results of VLBI measurements cannot be extracted from the model, since this would require that bins of milli-arcsecond (mas) size be used to study the angular distribution of the radiation, and in so many bins the Monte Carlo statistics would degrade very rapidly. These considerations will limit some of the discussion in this paper.

2 EXPLORATION OF OH MASER MODELS

2.1 Introduction

In Paper I, COHERENCE was applied to calculate the spectrum for a single model with realistic parameters. By calculating models for a range of parameters, one may attempt to constrain some of the physical properties of circumstellar 1612-MHz masers.

It is, of course, neither feasible to test all the dependences of the model, nor is it necessary. We limit ourselves here to some of the simple parameters that govern the radiative transfer in the shell; the overall geometry of the models is not changed. In particular, all models are spherically symmetric. The reason for choosing spherical symmetry is also practical: as was shown in Paper I, this allows averaging over all possible observers in all directions, thus decreasing the statistical fluctuations in the Monte Carlo models.

The spectra are determined by the radiative transfer of the maser, which depends on the distribution of OH inversions, $\Delta n_{\rm OH}(r)$. This is only a function of radius r for spherical symmetry, and is independent of time for a stationary solution. This number is determined by the stimulated emissions of the maser on the one hand and the product of density and pump rate, $\mathscr{R}_{12}(r) = n_{\rm OH}(r) P_{12}(r)$, on the other. When locally the OH density is increased in the model, the gain for passing rays will be larger, as the net population inversion is increased. The maser will therefore be stronger and may show a different spectrum as well. The true situation is more complicated, however, because by increasing the density the optical depth in the pump line will also increase, changing $P_{12}(r)$.

The value of $P_{12}(r)$ depends on the details of the maser pump. For the case of a radiative pump, it is a fixed number times the pump photon volume density. In COHERENCE we use a constant relative pump rate, P_{12}, which was estimated from a scheme in which the maser is pumped by infrared absorptions in the 35-μm line of OH (Paper I). Because the pump rate is fixed, changes in optical depth in the pump line with increasing density are ignored. This implies that a change in density results in a direct change of the total OH inversion rate $\mathscr{R}_{12}(r)$, which is a fundamental parameter for the solution of the radiative transfer in the present model.

All calculations are performed for homogeneous shells with a constant OH density between an outer and an inner radius. In the mass loss from the star we expect the total density to follow $1/R^2$, although the presence of OH is governed by chemical reactions and may deviate from this. We have found that a density profile roughly symmetric around an average radius is required to obtain realistic results. In particular, we have tried a profile that falls off with radius according to $1/R^2$ between two limiting radii. This greatly enhances the blueshifted peak in the OH profile, because the unsaturated core in the maser shifts closer to the centre of the shell. The simplest profile that satisfies the conditions is a constant-density profile (boxcar).

In all cases the geometric average radius, $R = (R_{\rm in} + R_{\rm out})/2$, of the shell is fixed at 3×10^{16} cm. The geometric mean radius is used because it equals the radius determined from the phase lag between the two extreme velocities. The expansion velocity is always set to 20 km s^{-1}. Both of these are arbitrary scaling parameters. Essential parameters are the ratio of shell thickness to radius and the ratio of velocity width to expansion velocity.

2.2 Results

In Fig. 1 we show a grid of models with different OH density [different $\mathscr{R}_{12}(r)$] and different shell thickness. The central panel represents the set of parameters that was presented in Paper I as the standard model. All other parameters are fixed in the models.

From Fig. 1 it is clear that towards the top of Fig. 1 the maser profiles get brighter. This is no surprise, because for thicker shells the total number of photons increases rapidly for a fixed pump rate. The total OH flux also increases somewhat with decreasing density. In addition, it appears that towards the right (and, although less pronounced, towards the top) the spectra appear slimmer. This is a result of increasing saturation and the associated effects of beam-crossing for models with lower $n_{\rm OH}$ (and larger shell thickness ΔR), which implies that, at some position in the shell, fewer excited molecules are available for amplification of the maser emission. As explained in Paper I, this enhances the anisotropy of the maser emission, thereby increasing the flux of the peaks and limiting the 'inner parts' of the spectrum.

It is not clear whether the presence of slight asymmetries between the red- and blueshifted peaks in some of these models is an artefact of the code. Some asymmetries may arise from the way in which grid cells are implemented throughout the shell, but they may also originate from the adopted density profile, which enhances the saturation in the

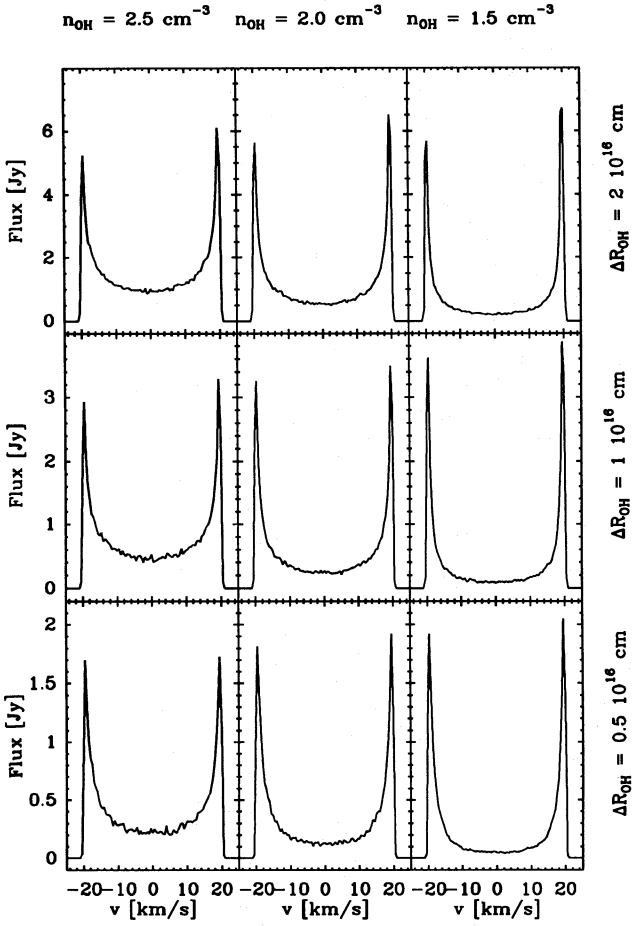

Figure 1. Grid of a few models with changing shell thickness and temperature.

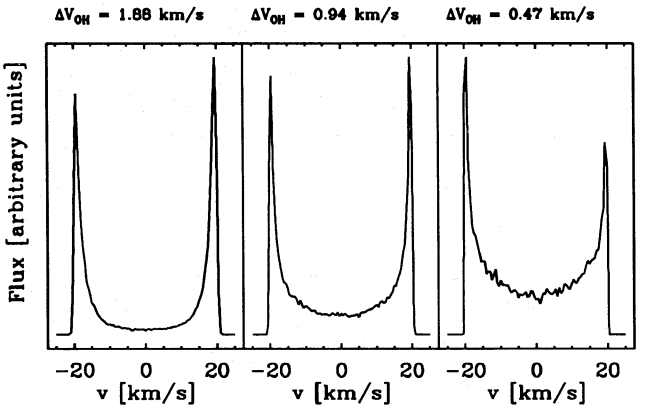

Figure 2. Spectra for different values of ΔV: from left to right, $\Delta V_{\rm OH} = 1.88$, 0.94 and 0.47 km s^{-1}.

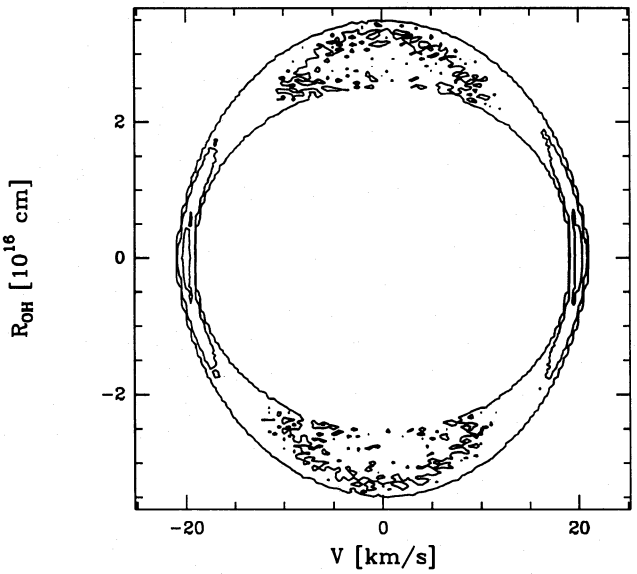

Figure 3. The radial brightness distribution in different velocity channels for the standard model.

inner shell and favours the redshifted peak in the same way as the blueshifted peak was favoured in density distributions with a $1/R^2$ dependence (see above).

These simulations show that with a fixed pump rate the appearance of the line profile changes significantly for relatively small density-variations. This does not necessarily imply that real astrophysical masers are sensitive to changes in the OH abundance, because it is really $\mathscr{R}_{12}$ that is changed. This net pump rate will in realistic cases not increase with density, but is fixed by the amount of infrared photons present. This is confirmed in models where the pump rate is not fixed; in such experiments all spectra look similar and only the strength of the maser varies.

The velocity width of the OH molecules in these models can also be changed. In the standard model the OH molecules have $\Delta V \approx 1$ km s^{-1} (FWHM), corresponding to a temperature of more than 300 K. As was argued in Paper I, this does not seem realistic from estimates of the temperatures in circumstellar shells, and is probably related to turbulence in the gas shells. Spectra for different values of the width of the velocity distribution are shown in Fig. 2.

It turns out that the models are relatively sensitive to this parameter, but of course, this range in ΔV represents a very large range in kinetic temperature or turbulence. For broader OH velocity distributions, the maser finds more coherent paths in the medium, and therefore the maser is more saturated. This implies relatively less flux in the inner channels of the spectra, so an increase of the velocity width enhances the strength of the peaks relative to the centre. It is clear that for small velocity-width the blueshifted peak is substantially stronger than the redshifted one. It may be that the small velocity-width results in substantial gain only near the outer edge of the shell, which thus favours blueshifted radiation.

3 EFFECTS ON PHASE-LAG DISTANCES

From the models, the brightness distribution as a function of projected radius can be calculated for each velocity channel. These brightness distributions can then be compared with channel maps of high-resolution observations. We show in Fig. 3 the results for a model with the standard parameters in a velocity and projected-radius diagram. As expected, the peaks of the spectra come from confined regions, which correspond to the front and back of the shell. It is also clear that at other velocities the maximum of the emission lies near the outer edge of the shell. This may depend on the chosen density profile.

The measurement of distances to OH/IR stars with the phase-lag method is based on a comparison of the apparent angular size and a measurement of the phase lag. How the phase lag appears in the case of non-isotropic emitting shells is discussed below. First we concentrate on the apparent shell size.

3.1 The apparent angular size

Because we see different parts of the shell at different velocities in the spectrum, we expect the apparent size of the shell (Y_v, see Fig. 4) to change with v according to

$$Y_v = R_v \sqrt{1 - \frac{v^2}{v_{\exp}^2}}. \quad (1)$$

The first assumption entering the determination of the size is that the shell is spherically symmetric. Secondly, it is generally (or indeed implicitly) assumed that $R_v = R$, i.e. that at every observed velocity the emission originates at the same distance from the star. In that case, R can be estimated from measurements of Y_v. We can check this procedure in our models: emission in each direction does not necessarily originate at the same diameter, and hence generally $R_v \neq R$.

We plot in Figs 5 and 6 an estimate of the radius at each velocity, $\hat{Y}_v$, and compare it with the geometric mean radius of the density distribution in the model (R). Both figures are derived from one model calculated with the standard values, but $\hat{Y}_v$ is determined in two different ways. In Fig. 5 we use the first moment of the brightness distribution to find the angular size of the model shell. In Fig. 6 we use the position of the maximum flux density. The latter method probably approaches more closely the procedure of estimating the size of the shell from synthesis mapping, because interferometers are generally more sensitive to the detection of isolated features.

We see a small effect in Fig. 5 and a much larger one in Fig. 6: the radius determined from the brightness distribution is systematically larger than the mean radius of the density distribution. The explanation must be that the tangential maser gains are larger near the outer radius. The difference is much greater when the position of the maximum is used, because the radial intensity distribution is quite asymmetric. We have carried out the same experiment for masers that are more saturated or have thicker shells. In these masers, the peaks are more pronounced and the effect increases.

In Figs 5 and 6 an estimate of the apparent width of the brightness distribution is also given. This is again measured from the models. In the case where the mean radius is calculated from the first-order moment, the FWHM is derived from the second-order moment. For Fig. 6 the width at half-power is displayed. As expected, we find that the apparent thickness of the shell is less than the width of the density distribution, as a result of the beaming of the radiation.

The results have been obtained with a model with constant density distribution between inner and outer radii, and this is not necessarily a very representative situation.

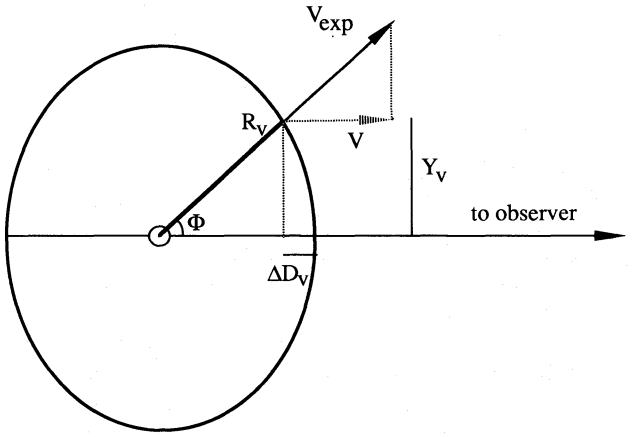

Figure 4. The geometry of the angular sizes and phase lags.

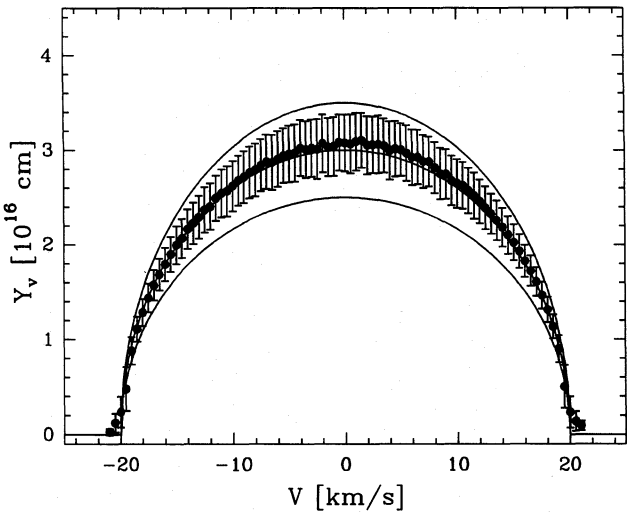

Figure 5. Measured radii Y_v from the model brightness distribution, measured by taking moments. Dots indicate the radii, bars are FWHM sizes. The lines indicate the inner, outer and mean radii of the density distribution.

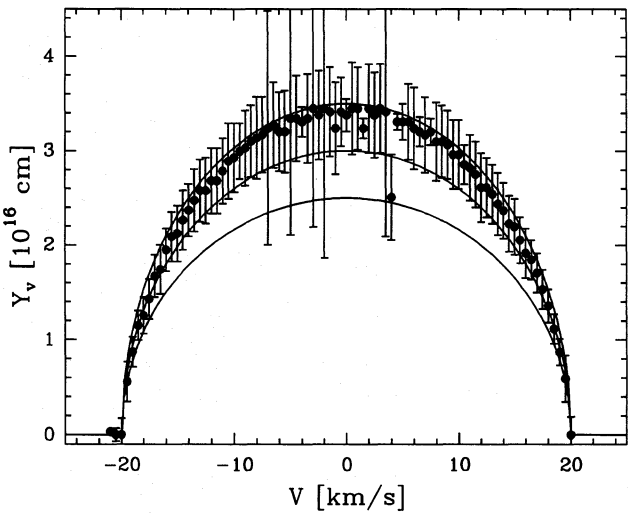

Figure 6. Measured radii Y_v from the model brightness distribution, measured by taking the position of the maximum flux density. Dots indicate radii; bars are FWHM sizes. The lines indicate the inner, outer and mean radii of the density distribution. The large scatter in this diagram is a result of the fact that the position of the maximum is relatively sensitive to noise.

Moreover, in the analysis of actual observations one is usually limited to the outer velocities: at the stellar velocity, where the angular size is a maximum, the fluxes are at their lowest values and quite often an interpolation of the angular size through the inner region has to be made.

3.2 Effects on the phase lag

The measurements of the angular sizes of circumstellar shells, combined with phase-lag measurements, have been used to determine distances to these objects (Herman & Habing 1985b; van Langevelde et al. 1990; West et al. 1992; Chapman et al. 1993). A phase lag can be measured between the redshifted and blueshifted parts of the spectrum when the variability of the star is accurately monitored. This variability originates from the bolometric variations of the star, and these variations are transferred by the circumstellar dust to the OH, by means of variations in the pump. Because the near side of the shell (blueshifted peak) is about 30 light-day closer to the observer than is the back side, a traveltime difference between the peaks becomes apparent.

We can look at the situation in terms of the way in which the signal of the variations is transferred from the star to the observer. First, the signal travels in a radial direction specified by the angle ϕ. At some radius R_ϕ this pumps the maser. We observe the radiation coming from this radius at a certain velocity in the spectrum, because of the Doppler shift of the projected velocity. The maser is observed after the signal has travelled the distance D to the observer plus ΔD_ϕ, the surplus depth along the line of sight. The difference in travel-distance gives rise to the phase lag, τ_ϕ, with respect to the blueshifted peak ($\phi = 0$); we can write (see Fig. 4)

$$\tau_\phi c = (R_\phi - R_0) + (R_0 - R_\phi \cos\phi) = R_\phi(1 - \cos\phi). \quad (2)$$

Generally, this result is expressed in terms of v, the observed velocity in the spectrum, rather than ϕ. According to Fig. 4, we write

$$\tau_v c = R_v\left(1 + \frac{v}{v_{\exp}}\right). \quad (3)$$

We see that the phase lag for the blueshifted peak equals zero, and that when we adopt $R_v = R$ the phase lag increases linearly over the spectrum to a maximum value of $2R$. For $R_v \neq R$, therefore, a different relation may arise. From the brightness distribution we can estimate the radius R_v for all but the outermost velocities. In this way, estimates of τ_v are obtained. These are shown in Fig. 7 and compared with the simple case when $R_v = R$.

There appears to be a small effect in the phase lag, namely that the simple method overestimates the size of the shell. Caution is required, however, because in the determination of the phase lag the emission at the outer velocities usually has highest weight, first because these channels have the best signal-to-noise ratio, and secondly because between the outer velocities the phase lag appears with maximum value. At these outer points, R_v cannot be measured from a (Y_v, v) distribution and our method breaks down. It is not straightforward how one should estimate the phase lag between the most extreme peaks in the spectrum for a geometrically thick, masering shell. The signal through the near-shell travels undelayed, so we only have to estimate at what radius

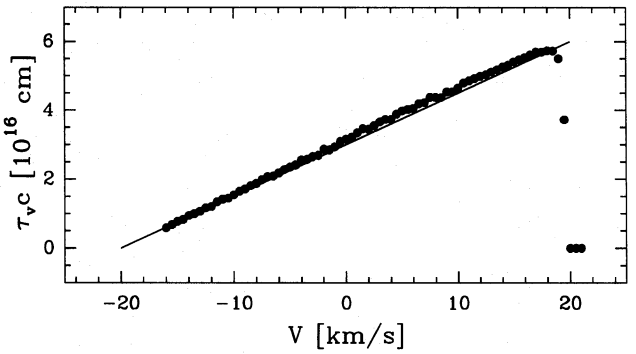

Figure 7. Phase lags from the models. The solid line represents the linear increase of the phase lag for $R_v = R$.

at the far side the infrared signal is converted into a 1612-MHz signal to the observer. Insight on this can be obtained when we address the question at which moment the maser output will reach a maximum in response to a slowly varying pump signal. For a saturated maser, this must be at the moment at which the maximum infrared emission has reached the geometrical mean, because then the largest number of photons over the integrated thickness of the shell are available. Thus we argue that the phase lag between the extreme velocities must equal $2R/c$.

3.3 Discussion

It has been shown that a non-isotropic effect may exist that affects the measurement of the angular sizes of OH/IR stars. This leads to an overestimate of the angular size and thus to an underestimate of the distance when $R_v = R$ is assumed, but such a bias is small ($\leq$10 per cent) for the standard model. It is larger in models with thicker shells or in models in which the maser is more saturated.

The same effect is expected to be present in the phase lag, but is not as pronounced. We expect the phase lag in the inner part of the spectrum to appear larger than the lag between the two outer peaks. In other words, the inner spectrum on the redshifted side has a small extra delay in comparison with the blueshifted peak. The reason for this is that the emission in the inner parts of the spectrum originates from the outer edge of the shell. In practice, it is usually only the phase lag between the outer spectral features that is measured, and hence the effect on the distance estimate is small. We therefore predict a net small systematic error of $\leq$10 per cent in OH/IR distance measurements for which this effect is neglected.

4 AMPLIFIED STELLAR RADIATION

4.1 Introduction

Several observations have revealed the presence of very compact maser spots in the blueshifted peaks of OH/IR stars (Norris et al. 1984; Sivagnanam et al. 1990), and very high brightness temperatures in the blue peak. This is explained as the amplified emission from the stellar continuum. The observations by Sivagnanam et al. (1990) provide a particularly strong indication, because they show that the positions of such maser spots in two different OH transitions coincide to within 7 mas. This has given rise to controversy, because it

has been argued that in a saturated maser the radiation output is determined by the volume-integrated pump rate and thus cannot be affected by the 1612-MHz photons from the star that lies behind the masering medium. The equations of radiative transfer (Paper I) show that this is only partly true. The J_ν-term is fixed for saturated masers; the production is limited by the pump rate, but the intensities are not fixed. A background source can trigger the induced emission, and this may collimate radiation in a certain favourable direction. It turns out that, for a shell at 3×10^{16} cm, the contribution of 1612-MHz photons coming from an asymptotic giant branch (AGB) star is small compared with the spontaneous emission: at 2000 au even a 1-au AGB giant is reduced to a small, ≤ 2 arcmin, object in the sky. The relative contribution to photons travelling radially is not negligible, however, but comparable to spontaneous emissions.

The next question is whether this small contribution from the star can influence the radiation field. It is not practical to study this in a spherical grid, in which we calculate a solution for the whole global radiation field. Instead, we have created a version of COHERENCE that uses a rectangular grid. This should resemble a radial portion of the shell. The size of the slab is estimated from the standard model. The long axis equals the thickness of the shell (10^{16} cm), while the short axis is set to the dimension of a region in which all OH molecules have comparable velocities, and so is determined by the width of the velocity distribution. From these considerations, an axial ratio of 1:7.5 is estimated.

We point out that by using this small slab we do not reproduce the full radiative transfer in the circumstellar shell, but it will be sufficient to study the existence of an amplified stellar image. We use the parameters from our standard model. The stellar emission is calculated as resulting from a 5000-K blackbody which illuminates the two middle cells of one side of the rectangular grid. The initial direction of these 1612-MHz photons is always radial, i.e. precisely along the longest axis of the rectangular grid.

4.2 Results

In Fig. 8 we show the results for a simulation with and without a stellar source, where the angular dependence of the intensity integrated over the cells at the short side opposite the star is shown. The difference between the two simulations (for which the difference in J_ν is negligible) is a strong feature which is contributed by the middle two cells. The spike is quite strong but also quite narrow. This is expected: higher intensities will be beamed more strongly. In the model the maser was saturated. The resolution of our code is not sufficient to compare our results directly with VLBI measurements. To obtain the appropriate angular resolution we would have to bin our data in 20-mas bins, and that would certainly reveal the individual photon packages used in the code. Nevertheless, the conclusion that there is a difference between the two cases remains valid.

It is interesting to see what the effect of a changing axial ratio is on the amplified stellar image. While the short axis remains fixed, the long axis is increased. This represents an increase in shell radius. As expected, the maser becomes more saturated, making the effect of the amplified stellar image less pronounced, because the ratio of spontaneous photons to photons from the background decreases. However, the effect remains detectable. It could well be that in true masers the spot becomes more confined and of higher brightness temperature, but COHERENCE cannot follow these details.

5 CONCLUSIONS

Monte Carlo simulations of circumstellar 1612-MHz OH masers show that a wide range of parameter values produces the characteristic two-peaked OH spectrum. This is satisfying, because masers occur in a large fraction of the sources (≈ 90 per cent: Gaylard et al. 1989).

It is clear from the apparent brightness distribution of the models that the emission in velocity channels close to the stellar velocity originates from the outer radii of the shell. This biases measurements of the angular size of the circumstellar shell. A similar effect is present in the phase lags, but this will not influence the phase-lag measurements much, because the effect disappears at the outer edges of the spectrum which are mostly used in phase-lag determinations. Our conclusion is that distances from phase-lag measurements may be underestimated by ≤ 10 per cent, which is less than the observational uncertainty in the most accurate distance determinations with this method.

Finally, hotspots are found in the blueshifted peaks of OH spectra, which are a result of amplified 1612-MHz photons from the stellar continuum. These modify the brightness temperatures in the blueshifted peaks by enhancing the

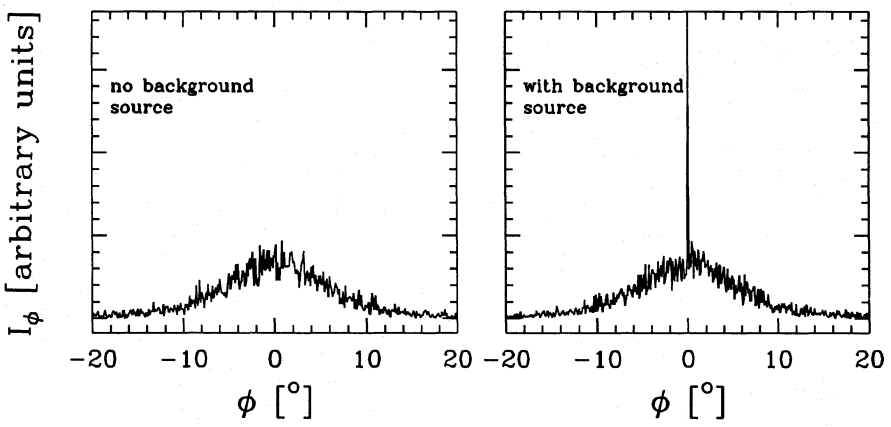

Figure 8. Output from a rectangular grid without and with a background source.

beaming of the radial emission. This does not imply that the flux densities of blueshifted radiation are on average higher.

REFERENCES

Chapman J. M., Killeen N. E. B., te Lintel Hekkert P., Caswell J. L., Harnett J., 1993, in Clegg A. W., Nedoluha G. E., eds, Astrophysical Masers. Springer-Verlag, Berlin, p. 345

Cohen R. J., 1989, Rep. Prog. Phys., 52, 881

Elitzur M., 1992, ARA&A, 30, 75

Elitzur M., Goldreich P., Scoville N., 1976, ApJ, 205, 384

Gaylard M. J., West M. E., Whitelock P. A., Cohen R. J., 1989, MNRAS, 236, 247

Herman J., Habing H. J., 1985a, Phys. Rep., 124, 255

Herman J., Habing H. J., 1985b, A&AS, 59, 523

Netzer N., Knapp G. R., 1987, ApJ, 323, 734

Norris R. P., Booth R. S., Diamond P. J., Nyman L. A., Graham D. A., Matveyenko L. I., 1984, MNRAS, 208, 435

Sivagnanam P., Diamond P. J., Le Squeren A. M., Biraud F., 1990, A&A, 229, 171

Spaans M., van Langevelde H. J., 1992, MNRAS, 258, 159 (Paper I)

van Langevelde H. J., van der Heiden R., van Schooneveld C., 1990, A&A, 239, 193

West M. E., Gaylard M. J., Combrick W. L., Cohen R. J., Shepherd M. C., 1992, in Warner B., ed., Variable Stars and Galaxies: a symposium in honour of Michael W. Feast. Astron. Soc. Pacif., San Francisco, p. 227